Journal of Electroanalytical Chemistry 744 (2015) 77–84

Contents lists available at ScienceDirect

Journal of Electroanalytical Chemistry

journal homepage: www.elsevier.com/locate/jelechem

Understanding the interaction of thiosulfate with Alloy 800 in aqueous chloride solutions using SECM

Da-Hai Xia [a], Ren-Kang Zhu [a], Yashar Behnamian [a], Jing-Li Luo [a,*], Chang-Jian Lin [b], Stan Klimas [c]

[a] Department of Chemical and Materials Engineering, University of Alberta, Edmonton, Alberta T6G 2G6, Canada
[b] State Key Laboratory of Physical Chemistry of Solid Surfaces, and Department of Chemistry, College of Chemistry and Chemical Engineering, Xiamen University, Xiamen 361005, China
[c] Atomic Energy of Canada Ltd, Chalk River Laboratories, Stn. 80, Chalk River, Ontario K0J 1J0, Canada

ARTICLE INFO

Article history:
Received 5 November 2014
Received in revised form 27 February 2015
Accepted 3 March 2015
Available online 5 March 2015

Keywords:
Alloy 800
Chloride
Thiosulfate
SECM
STM
EIS

ABSTRACT

In situ scanning electrochemical microscopy (SECM) and scanning tunneling microscopy (STM) assisted scanning reference electrode technique (SRET) were applied for the first time to study the interaction of thiosulfate with Alloy 800 surfaces in aqueous chloride solutions. Electrochemical impedance spectroscopy (EIS) and scanning electron microscope (SEM) were also performed to understand the interaction mechanism. The results showed that the effect of 0.075 mol/L thiosulfate in 0.6 mol/L chloride solutions strongly depended on the potential. There was no aggressive effect at the corrosion potential where the passive layer was intact, but a combined effect was observed with the presence of chloride ions at high potential where the passive layer was broken down.

1. Introduction

Alloy 800 is one of the materials used for steam generator (SG) tubing in CANDU®™ (CANada Deuterium Uranium) nuclear power stations and is also used in other pressurized water reactor (PWR) SGs due to its proven excellent corrosion resistance [1–3]. However, impurities on the SG boiling side, such as sulfate, chloride and lead, may collectively cause passivity degradation of Alloy 800 [4]. Sulfate concentrations measured in the SG blowdown could be up to 10 μg/kg, the concentrations of non-volatile impurities at the hideout in crevices may increase by several orders of magnitude. Moreover, sulfate may reduce to lower valence species such as H_2S, elemental S and $S_2O_3^{2-}$ under SG operating conditions; these species can be the powerful thermodynamic activators for copper, nickel, and iron through the formation of solid sulfide phases at more active (negative) electrochemical potentials than those at which the oxides form [5]. Thiosulfate ($S_2O_3^{2-}$) is known to cause accelerated corrosion of SG tubing materials [6], and more severe effects if other ions (such as Cl^-) are present [7–9]; however, the interaction of thiosulfate with the passive film in the presence of chloride ions is unknown.

In recent years, scanning electrochemical microscopy (SECM) has been developed for a wide range of applications in corrosion science [10–12]. An advantage of SECM is its capability to probe charge transfer occurring nonuniformly at interfaces [13,14]. Scanning reference electrode technique (SRET) has been used for determination of the potential distribution on corroding surfaces [15–20] and scanning tunneling microscope (STM) is a technique to study corrosion at micro- and nano-scale [21–24]. Zhu et al. [10] investigated the impact of tensile and compressive stress on reactivity of the Alloy 800 C-ring sample using SECM and found that both tension and compression increased the localized surface reactivity, indicating corrosion susceptibility of Alloy 800 under stress in thiosulfate-contained chemistries. Lu et al. [25] investigated the pitting and stress corrosion cracking of welded austenitic stainless steel using in situ scanning reference electrode technique (SRET). Mott–Schottky measurements were also used to investigate the electric properties as well as the susceptibility to the presence of chloride ions and tensile stress of passive films. Marcus et al. investigated the passive film growth mechanism at nano scale using STM combined with molecular dynamics simulation [22,23,26–29]. Limited studies of thiosulfate–chloride induced passivation degradation were performed using a combination of techniques [10].

In this work, the passive film on Alloy 800 was studied by SECM, STM assisted SRET, and EIS to observe the corrosion of Alloy 800 in thiosulfate–chloride solutions.

---

* Corresponding author.
E-mail address: jingli.luo@ualberta.ca (J.-L. Luo).

http://dx.doi.org/10.1016/j.jelechem.2015.03.006
1572-6657/

2. Experimental

2.1. Sample preparation

A specimen of Alloy 800 was cut from commercial tubing (Sandvik, heat number 516809) with a 15.88 mm outer diameter (OD) and an average wall thickness of 1.13 mm. After spot-welding copper wires to the internal surfaces, the specimens were then mounted in epoxy resin. Each specimen was polished with wet silicon carbide papers (Buehler Ltd.) in the sequence of 320, 600, 800, and 1200 grit, then rinsed copiously with deionized water, acetone and ethanol before drying in air. Surface roughness is less than 1um because the Alloy 800 is well-grounded. The composition of Alloy 800 used in the experiments is listed in Table 1. Fig. 1 shows the microstructure of the Alloy 800 using optical microscopy (OM) and the fully annealed equiaxed-grain optical microstructure of this alloy after etching with Marble's agent (10 g copper(II) sulfate, 50 mL concentrated HCl and 50 ml water) for 15 s.

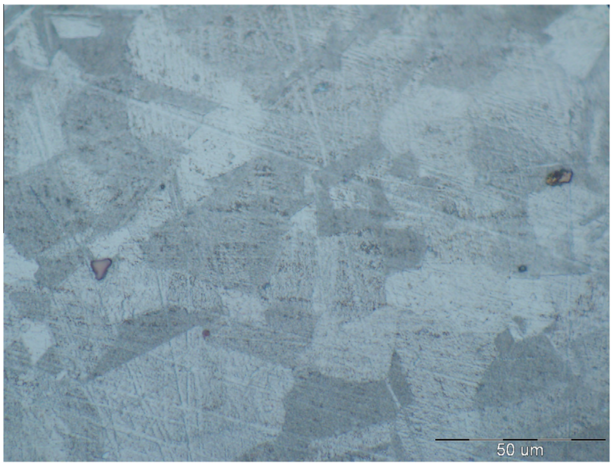

Fig. 1. Microstructure of Alloy 800 with an average grain size 20 μm after etching with Marble's agent (10 g copper(II) sulfate, 50 mL concentrated HCl and 50 ml water) for 15 s.

2.2. Scanning electrochemical microscopy

The surface reactivity was mapped by SECM. The electrolyte contained 0.9 mmol/L ferrocenylmethanol (99%, Aldrich) as the redox mediator and 0.6 mol/L sodium chloride (Fisher, reagent grade, >99%) with or without 0.075 mol/L sodium thiosulfate (Fisher reagent, >99%) as the supporting electrolyte. Deionized water (Milli-Q, Millipore, 18.2 MΩ cm resistivity) was used to prepare all solutions. During the SECM experiments, an epoxy-mounted specimen was sandwiched between two blocks of PTFE to form a cell. This cell was mounted on the SECM stage (CHInstruments, USA). An ultramicroelectrode (UME) with a radius of 10 μm and RG of 5 was used as the SECM probe. An Ag/AgCl electrode (saturated with KCl, CHI) was used as the reference electrode (RE) and a Pt wire was the counter electrode (CE). The potentials in this paper are presented in Saturated Calomel Electrode (SCE) scale. The probe was biased at a potential of 0.65 V_{SCE} until steady-state current was obtained, and then the probe was driven to the specimen surface in order to accurately determine the gap distance between the probe and the specimen. When the UME current (i_T) reached the prescribed value, the tip stopped automatically. The normalized current (I_T, the measured tip current divided by the tip current measured in bulk solution) vs. the normalized distance (L, the distance between the tip and specimen divided by the radius of UME) was plotted as the probe approach curve (PAC). The real gap distance between the tip and the specimen was estimated by comparing experimental PACs with simulated/theoretical PACs, as shown in the previous work [13,30–33]. The UME gap distance was maintained at constant and scanned above the specimen to obtain the SECM images of the Alloy 800 surface. The passive film exhibits semiconductor properties, and it was considered to be an inactive film. A diagram illustrating the SECM measurements is given in Fig. S1. The model we used is developed by Renkang Zhu and Zhifeng Ding [13]. SECM was performed at the constant-distance mode.

2.3. Scanning tunneling microscopy assisted scanning reference electrode technique

The potential mapping and STM imaging were performed using an XMBY2012 Scanning Electrochemical Workstation which is able to in situ image the potential distribution and topography simultaneously at the metal surface during the time period when the sample undergoes localized corrosion. The schematic diagram and the photograph of the system are shown in Fig. S2(a) and (b). The same platinum–iridium (Pt–Ir) probe was used as the scanning probe in both SRET and STM modes. The STM signal was employed to control the distance between the probe tip and the sample surface for the SRET measurement. The procedure consisted of two steps: (1) approaching the probe in STM mode until tunneling current was sensed (estimated to be no more than 1 nm from the surface [18]) and (2) withdrawing the probe away from the surface to the desired distance of 50 μm. In the SRET mode, the potential difference was mapped between the scanning Pt–Ir probe (E_{probe}) and another Pt–Ir electrode (E_{ref}). This reference electrode was positioned about 2 mm away from the surface. An image of the standard grating verified the instrument resolution and reliability [Figure S2(c)].

2.4. Potentiodynamic polarization and electrochemical impedance spectroscopy

Potentiodynamic polarization was applied by sweeping the potential in the positive direction at 0.1667 mV/s until the current density reached 1 mA/cm^2. The electrochemical measurements were performed using a Gamry (PC-750) electrochemical workstation. A three-electrode cell was used with the Alloy 800 specimen as the working electrode (WE), a SCE as the reference electrode and a platinum CE. EIS measurements were performed for each sample after immersing in solution for 12 h at the corrosion potential (E_{corr}). The applied superimposed signals had a 10 mV amplitude and a frequency ranging from 100 kHz to 0.01 Hz.

3. Results

3.1. Potentiodynamic polarization

Fig. 2 shows the anodic potentiodynamic polarization curves for Alloy 800 in different solutions at a scan rate of 0.1667 mV s^{-1} and

Table 1
Elemental composition of Alloy 800 (wt%).

C	Si	Mn	P	S	Cr	Ni	Co	Ti	Cu	Al	N	Fe
0.017	0.46	0.5	0.012	0.001	21.87	32.78	0.01	0.48	0.02	0.29	0.016	43.2